



Parameters controlling weld bead profile in conduction laser welding



W.A. Ayoola, W.J. Suder*, S.W. Williams

Welding Engineering and Laser Processing Centre, Cranfield University, MK43 0AL, United Kingdom

ARTICLE INFO

Keywords:

Conduction laser welding
Weld bead profile
Interaction parameters
Beam diameter

ABSTRACT

In laser welding and other processes, such as cladding and additive manufacturing, the weld bead geometry (depth of penetration and weld width) can be controlled with different parameters. A common practice is to develop process parameters for a particular application based on an engineering approach using the system parameters i.e. laser power and travel speed. However, in such a case the process is optimised for a particular system only. This study is focused on understanding of the phenomena controlling the weld profile in conduction welding for a wide range of beam diameters from 0.07 mm to 5.50 mm. It has been shown that the weld bead geometry can be controlled by the spatial and temporal distribution of laser energy on the surface of workpiece, such as power density, interaction time and energy density. This means that similar depths of penetration can be achieved with various optical set-ups. It has been also found that it is more difficult to achieve pure conduction welds with small beam diameters, which are typically used in powder bed additive manufacturing, due to high conduction losses and low vaporisation threshold.

1. Introduction

The weld profile, i.e. penetration depth and width of the fusion zone is the main parameter that laser users wish to control in any laser processing. In welding the processing conditions are selected based on the thickness of the material that has to be welded. In other processes, such as laser cladding or additive manufacturing, the required thickness of the deposited layer and the level of necessary dilution determine the penetration required by the process and the energy needed from the laser. Therefore, similarly to welding, in those processes the melt pool size determines dimensions of deposited features, which means that the laser energy has to be accurately controlled to achieve required dimensional accuracy and resolution.

In laser welding the same energy can be applied with different beam diameters, resulting in different spatial distributions of the heat in the workpiece, which will lead to different weld profiles. Beam diameter is one of the most important parameters determining the fusion characteristics and welding regime in laser processing. [Buvanashakaran et al. \(2009\)](#) showed that depending on the power density, different welding regimes occur in laser processing, identified as keyhole and conduction. According to [Assuncao et al. \(2012\)](#) there is a narrow window where pure conduction regime can be achieved, which depends on the power density and spot size. The keyhole regime is more common due to high aspect ratio weld profiles and hence high productivity and low distortion. However, the vaporisation, which is the inherent feature of the keyhole regime, increases the likelihood of

defects and, therefore in some critical applications conduction regime is a better choice. In the conduction regime no vaporisation should occur and the energy is transferred to the material from the surface via conduction, which results in a more stable melt pool and better surface finish. [Sanchez-Amaya et al. \(2009\)](#) showed that relatively deep penetration welds with smooth beam profile could be achieved in conduction regime. It is believed that in powder bed additive manufacturing vaporisation should be avoided to minimise the likelihood of defects, therefore the powder fusion should ideally be carried out in the conduction regime.

Many authors tried to optimise the process parameters to achieve good weld profiles. As shown by [El-Batahgy, \(1997\)](#) the weld profile is highly dependent on the laser power, welding speed and focal distance. [Benyounis et al. \(2005\)](#) adopted statistical approach to correlate welding parameters and the resulting weld profiles. [Moradi and Ghoreishi \(2011\)](#) expanded this to include defects, such as undercut and undesirable root profiles. However in this approach there is a risk that the process is optimised only for a particular machine and a particular material. In reality any change of a system parameter affects the fundamental laser material interaction parameters, which determine how the material perceives the heat source, and which then transpires into the resulting thermal cycle. Several authors tried to optimise laser welding based on the spatial and temporal distribution of energy of a laser source. Based on modelling it was shown that the rate of vaporisation of alloying elements is determined by the heat flux, as presented by [Mundra and Debroy \(1993\)](#). In another work [Fuerschbach and Eisler](#)

* Corresponding author.

E-mail addresses: w.a.ayoola@cranfield.ac.uk (W.A. Ayoola), w.j.suder@cranfield.ac.uk (W.J. Suder), s.williams@cranfield.ac.uk (S.W. Williams).

<http://dx.doi.org/10.1016/j.jmatprotec.2017.06.026>

Received 30 August 2016; Received in revised form 8 June 2017; Accepted 19 June 2017

Available online 20 June 2017

0924-0136/ © 2017 The Authors. Published by Elsevier B.V. This is an open access article under the CC BY license (<http://creativecommons.org/licenses/by/4.0/>).

(2002) showed the influence of pulse energy and interaction time on the weld pool size. Bag et al. (2009) achieved good agreement between a computational model and experimental welds for the same power density and interaction time. In another work Mecco et al. (2013) used power density and interaction time to characterise the thickness of an intermetallic layer of dissimilar laser welds. Suder and Williams (2012) studied interaction parameters that control the weld profile in keyhole welding. They demonstrated that the power density and specific point energy control the depth of penetration and the interaction time controls the weld width, independent of the optical set-up. This led to the formulation of the power factor, a phenomenological model, which enables transfer of data between lasers with different beam diameters developed by Suder and Williams (2014).

Motivated by these studies, the current work is focused on characterisation of the weld bead profile in laser conduction welding, in terms of fundamental laser material interaction parameters. The objective is to find parameters that control the weld bead geometry for a wide range of beam diameters. Conduction regime is beneficial in high quality welding applications and additive manufacturing, therefore this regime is the particular interest of this work. The effect of beam diameter is studied with consideration of the spatial energy distribution and its effect on the weld profile.

2. Experimental procedure

Most of the experiments were carried out using an IPGYLR-8000 continuous wave (CW) fibre laser with a maximum output power of 8 kW. The laser beam delivery system consisted of an optical fibre with a core diameter of 300 μm and a processing head with an optical magnification of two. The laser was used at the focal point, which resulted in a beam diameter of 610 μm , and also in out-of-focus position to achieve beam diameters between 1 mm and 5.5 mm. To prevent the laser head from back reflection, it was tilted at 10° angle backwards to the welding direction. The beam diameters were measured using a rotating pin-hole beam profiler (Primes Focus Monitor). The intensity distribution profiles are shown in Fig. 1. The second order moment definition was used to define the beam diameter.

Additional welds were achieved using two additional laser systems. The first one was an SPI fibre laser with a maximum power of 500 W and an optical fibre with a core diameter of 50 μm , equipped with a processing head with an optical magnification of two. This system was used at the focal point, which resulted in a beam diameter of 100 μm . The second system was a commercial powder bed machine RenAM 250 M manufactured by Renishaw. Note that in this case no powder was used; just bead-on-plate welds on a steel substrate. The machine was equipped with a 200 W fibre laser and a galvo-scanner head for the beam delivery, which resulted in a beam diameter of 70 μm . This system was also used at the focal point. The beam diameter was measured using an edge-knife beam profiler according to the second order moment definition.

All experiments were carried out as bead-on-plate welds in S275 mild steel with 12 mm thickness in 1G welding position. Even in the case of the powder bed machine, no powder was used but bead-on-plate welds in a steel substrate were performed. The plates were cleaned with acetone prior to welding and coated with graphite to ensure constant absorptivity. The samples were clamped firmly and experiments were carried out without shielding gas. The samples were cross sectioned at the half-length of each weld, polished and etched with 2% Nital solution prior to macroscopic investigation.

2.1. Interaction parameters

In this study different interaction parameters characterising spatial and temporal distribution of the laser energy on the surface of work-piece were used, after Suder and Williams (2012) and Assuncao et al. (2012), as follows:

$$\text{Power density } P_d = \frac{4P}{\pi D_B^2} [\text{Wm}^{-2}] \quad (1)$$

$$\text{Interaction time } t_i = \frac{v}{D_B} [\text{s}] \quad (2)$$

$$\text{Specific point energy } E_{SP} = P_d \times t_i \times \frac{\pi D_B^2}{4} [\text{J}] \quad (3)$$

$$\text{Energy density } E_d = P_d \times t_i [\text{Jm}^2] \quad (4)$$

where P is laser power; D_B is beam diameter and v is welding speed.

2.2. Power density P_d and specific point energy E_{SP}

Firstly it was investigated if a constant power density and specific point energy controls the depth of penetration, as reported for keyhole welding by Suder and Williams, (2012). A set of experiments with different beam diameters was carried out. The laser power and travel speed were continuously adjusted to each beam diameter, according to Eq. (1) and Eq. (3), to maintain the power density and specific point energy constant, as shown in Table 1. Four different beam diameters and four different combinations of power density and specific point energy were used.

2.3. Power density (P_d) and interaction time (t_i)

In the next set of experiments constant power density and interaction time were tested. In each case a constant combination of power density and interaction time was set-up and the beam diameter was varied. The laser power and travel speed were continuously adjusted to the beam diameter, according to Eq. (1) and Eq. (2). This was repeated for four different interaction times between 60 and 480 ms and four different power densities between 20.4 and 28 kW/cm², as shown in Tables 2 and 3. At this stage big beam diameters were used to enable easier interpretation of the observed phenomena with large melt pools. Then after initial confirmation of the hypothesis, the experiment was expanded to a wider range of beam diameters from 1 mm to 5.5 mm, as shown in Table 4.

2.4. Calculation of melting energy and conduction losses

To evaluate the proportion of energy utilised for melting to the energy dissipated for conduction losses within the bulk of the material, an analytical solution of the heat equation after Ashby and Easterling, (1984) was used:

$$T(z, t) = T_0 + \left[\frac{(AP/v)}{2\pi\lambda [t(t+t_0)]^{1/2}} \right] \cdot \exp - \left(\frac{(z+z_0)^2}{4\alpha t} \right) \quad (5)$$

where, T_0 is room temperature; A is absorptivity; P is laser power; v is welding speed; λ is thermal conductivity, t is time, z is depth below surface; α is thermal diffusivity and t_0 is given by

$$t_0 = \frac{D_B^2}{16\alpha} \quad (6)$$

where, D_B is beam diameter. After differentiating Eq. (5) with respect to time and rearranging it, the peak temperature T_{peak} achieved in each thermal-cycle can be determined from Eq. (7), after Ashby and Easterling, (1984):

$$T_{peak} = T_0 + \frac{2A(P/v)}{e\pi\rho C_p(z+z_0)^2} \quad (7)$$

where, e is base of the natural logarithm, ρ is density, C_p is heat capacity and with z_0 given by

$$z_0 = \left[\left(\frac{\pi^{1/2}}{e} \right) \left(\frac{\alpha D_B}{2v} \right)^{1/2} \cdot \frac{D_B}{2} \right]^{1/2} \quad (8)$$

The energy utilised for melting can be calculated from the isotherm

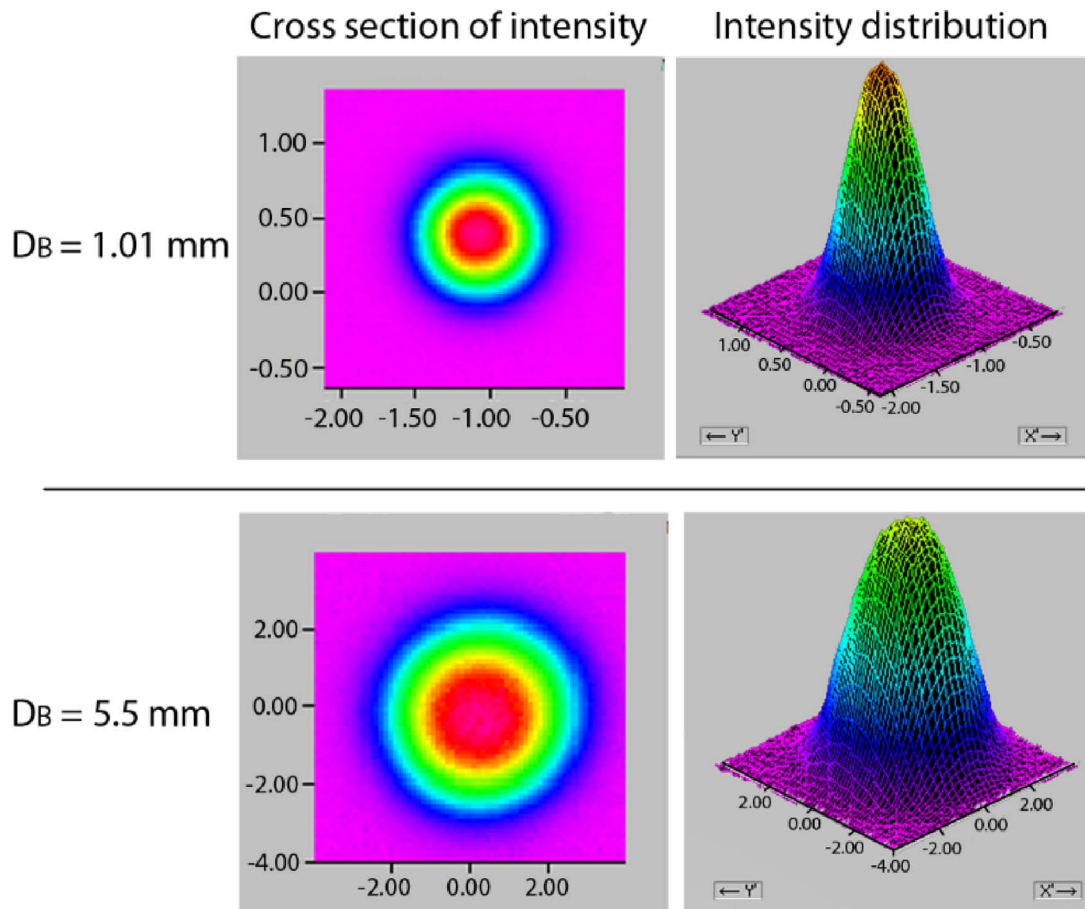


Fig. 1. Intensity distribution profiles of 1.01 mm and 5.5 mm beam diameters.

Table 1

Parameters used to investigate effect of beam diameter on weld profile at constant power density and specific point energy; (D_B – beam diameter, t_i – interaction time, v – welding speed, P – laser power).

D_B (mm)	t_i (ms)	v (mm/s)	41.5 kW/cm ² & 162 J P (kW)	55.1 kW/cm ² & 216 J P (kW)	64.0 kW/cm ² & 251 J P (kW)	75.0 kW/cm ² & 295 J P (kW)
1.01	480	2.00	0.34	0.45	0.52	0.62
1.44	240	6.00	0.68	0.90	1.04	1.22
2.04	120	17.00	1.36	1.80	2.09	2.46
2.87	60	47.70	2.68	3.56	4.14	4.86

Table 2

Parameters used to investigate effect of beam diameter on weld geometry at a constant power density of 28 kW/cm² and a range of interaction times; (t_i – interaction time, D_B – beam diameter, P – laser power, v – welding speed).

t_i (ms)	D_B (mm)	P (kW)	v (mm/s)
60	4.00	3.52	66.0
	5.00	5.50	83.3
	6.00	7.92	99.5
120	4.00	3.52	33.2
	5.00	5.50	41.7
	6.00	7.92	49.8
240	4.00	3.52	16.7
	5.00	5.50	20.8
	6.00	7.92	25.0
480	4.00	3.52	8.3
	5.00	5.50	10.4
	6.00	7.92	12.5

Table 3

Parameters used to investigate effect of beam diameter on weld geometry at a constant interaction time of 480 ms and a range of power densities; (P_d – power density, D_B – beam diameter, P – laser power, v – welding speed).

P_d (kW/cm ²)	D_B (mm)	P (kW)	v (mm/s)
20.4	4.00	2.56	8.3
	5.00	4.00	10.4
	6.00	5.76	12.5
22.9	4.00	2.88	8.3
	5.00	4.50	10.4
	6.00	6.48	12.5
25.5	4.00	3.20	8.3
	5.00	5.00	10.4
	6.00	7.20	12.5
28.0	4.00	3.52	8.3
	5.00	5.50	10.4
	6.00	7.92	12.5

Table 4

Parameters used to investigate effect of beam diameter on weld geometry at constant power density of 33.1 kW/cm² and interaction time of 120 ms (energy density of 4.0 kJ/cm²); (D_B – beam diameter, P – laser power, v – welding speed).

D_B (mm)	P (kW)	v (mm/s)
1.01	0.30	8.4
1.44	0.60	12.0
2.04	1.10	17.0
2.87	2.10	23.8
4.00	4.20	33.3
5.00	6.50	41.0
5.50	7.90	46.0

representing the melting point of a material based on the temperature distribution, as shown in Fig. 2 and given by:

$$E_{Melt} = \left[\frac{1}{2} \pi (z_{Melt}^2) \cdot l \rho \right] \cdot [C_p(T_M - T_0) + H_m] [J] \tag{9}$$

where, E_{Melt} is energy utilised for melting; z_{Melt} is depth of the melt zone; l is length of the weld; ρ is density; C_p is heat capacity; T_M is melting temperature, T_0 is room temperature and H_m is enthalpy of melting (latent heat).

In the same way the energy utilised for heating of the material but not contributing to the melting (conduction losses) can be calculated by summation of the areas for each temperature interval between the melting point and 200 °C (Fig. 2), according to

$$E_{Loss} = \sum \left[\left(\left(\frac{1}{2} \pi (z_{1400}^2 - z_{Melt}^2) \right) \cdot l \rho \right) \cdot (C_p(T_{1400} - T_0)) \right] + \left[\left(\left(\frac{1}{2} \pi (z_{1300}^2 - z_{1400}^2) \right) \cdot l \rho \right) \cdot (C_p(T_{1300} - T_0)) \right] + \dots + \left[\left(\left(\frac{1}{2} \pi (z_{200}^2 - z_{300}^2) \right) \cdot l \rho \right) \cdot (C_p(T_{200} - T_0)) \right] [J] \tag{10}$$

where, E_{Loss} is energy utilised for conduction losses; z_{1400} is the distance between the surface and the isotherm with a temperature of 1400 °C; T is temperature.

The ratio of conduction losses to the energy utilised for melting was calculated in the following way. Firstly Eq. (7) was used to calculate the temperature as a function of depth below the laser beam (Fig. 2). To simplify the calculations a uniform hemispherical weld profile was assumed. The melt depth was calculated based on the welding parameters used in the experiment from Fig. 9 and material properties given in Table 5. The melt depth was considered to

Table 5

Thermal properties used to calculate energy utilised for melting and conduction losses.

Symbol	Name	Unit	Value
T_0	Room temperature	K	298
ρ	Density	kg m ⁻³	7600
α	Thermal diffusivity	m ² s ⁻¹	1.1×10^{-5}
C_p	Heat capacity	J kg ⁻¹ K ⁻¹	510
e	Base of the natural logarithm		2.72
H_m	Enthalpy of melting	J kg ⁻¹	250,000

correspond to an isotherm of 1500 °C. The distance between the surface and the 1500 °C isotherm was assumed to be the molten metal (z_{melt}). Then the area of the melt pool (S_{melt}) was calculated, based on the melt depth (z_{melt}) with the assumption of a hemispherical weld profile from Eq. (9). The value of absorptivity in Eq. (7) was adjusted in each case to achieve the same melt area as in the experimental welds. In the next step, isotherms for temperatures between 1500° and 200 °C with an interval of 100 °C were determined from Eq. (7). The distance between isotherms of 1500 °C and 200 °C was assumed to be the conduction losses depth (z_{loss}). Based on this the area of each segment and the energy utilised in each temperature interval (S_{loss}) was calculated. Then the energies for each temperature interval were summed up and the total energy utilised for conduction losses was calculated using Eq. (10).

3. Results

3.1. Power density (P_d) and specific point energy (E_{Sp}) (Table 1)

Macrographs for these conditions are shown in Fig. 3. It can be seen that both the weld width and depth of penetration vary with the beam diameter, despite constant power density and specific point energy. The whole set is plotted in Fig. 4. It can be seen that the depth of penetration changes with the beam diameter. The same trend was observed for the whole range of power densities and specific point energies. This

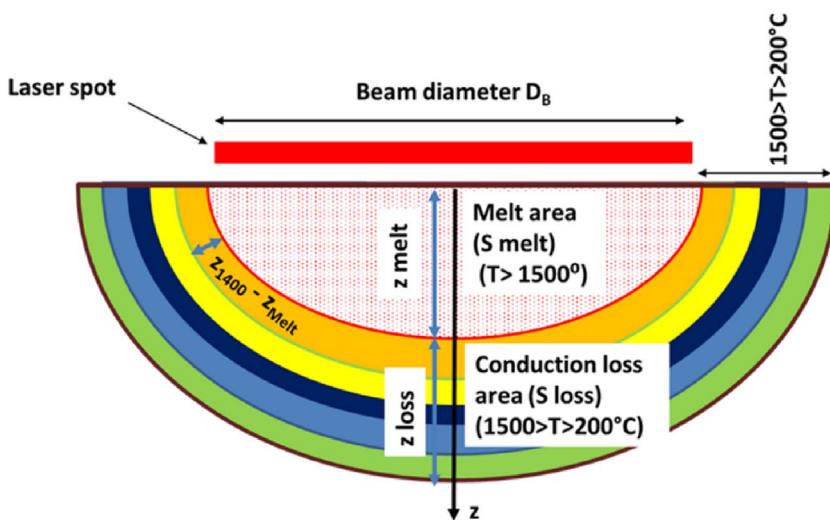


Fig. 2. Calculation of melt area and conduction loss area based on analytical solution of heat equation (Eq. (7)).

D_B (mm)	1.01	1.44	2.04	2.87
t_i (ms)	480	240	120	60

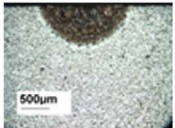
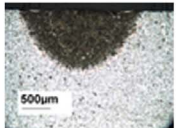
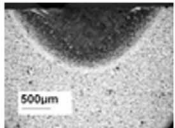
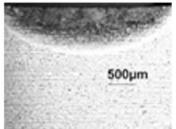
162 J & 41.5 kW/cm ²				
---------------------------------	---	---	---	--

Fig. 3. Macrographs at constant power density (P_d) and specific point E_{sp} for different beam diameters (D_B).

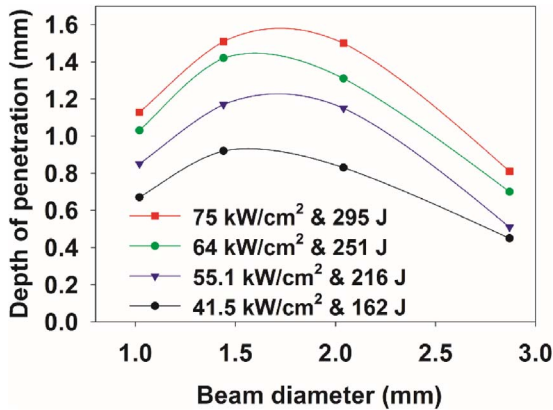


Fig. 4. Depth of penetration as a function of beam diameter at constant power density and specific point energy.

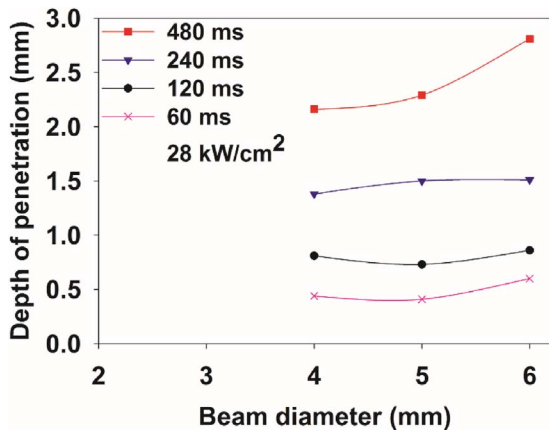


Fig. 5. Effect of beam diameter on depth of penetration at constant power density of 28 kW/cm² for a range of interaction times.

confirms that the conduction regime does not respond to the applied laser energy in the same way as in the keyhole regime.

3.2. Power density (P_d) and interaction time (t_i) (Table 2)

It can be seen in Fig. 5 that the depth of penetration is constant and only for the interaction time of 480 ms a discrepancy can be observed. In the case of 480 ms the depth of penetration increases with increasing beam diameter, despite constant power density and interaction time. In Fig. 6 macrographs of the corresponding data from Fig. 5 are shown. At 480 ms the weld profiles exhibit the aspect ratio greater than 0.4 indicating that the welds are in the transition regime. It is confirmed that, apart from the interaction time of 480 ms, the depth of penetration is proportional to the interaction time at constant power density and is independent of the beam diameter.

In Fig. 7 the same results are plotted as a function of interaction time. The depth of penetration increases almost linearly with increasing interaction time and is independent of the beam diameter. There is a discrepancy only for the interaction time of 480 ms. When compared to

the power density in Fig. 8, it can be seen that the effect of interaction time on depth of penetration is much greater than the effect of power density, which is typical for conduction regime with large beams. The slopes are 0.94 and 0.55 for the interaction time and power density respectively when the plots are normalised. This suggests that the weld profile in conduction regime is more dependent on the interaction time than on the power density, which is attributed to the time needed for the energy to transfer from the laser interaction point to the bulk of the material and generate melting.

To further test the effect of power density and interaction time on the weld profile, a wider range of beam diameters was used, as shown in Table 4. Beam diameters from 1 mm to 5.5 mm were used and constant power density and interaction time was achieved by adjusting the welding parameters for each beam. From macrographs presented in Fig. 9 it can be seen that initially the depth of penetration is dependent on the beam diameter and then at a certain point it becomes independent of it. The same trend was observed for a higher power density, as shown in Fig. 10.

The data from Figs. 9 and 10 is plotted in Fig. 11. For large beam diameters the depth depends on the power density and interaction time and is independent of the beam diameter. As the beam diameter is reduced below 3 mm the beam diameter has a significant effect on the depth of penetration. This suggests that the material response is also dependent on the size of the heat source, which links it to the specific point energy. The weld width, on the other hand, is entirely controlled by the beam diameter, when the power density and interaction time are maintained constant, as shown in Fig. 12. In all cases the weld width approached the diameter of laser beam projected on the workpiece.

To understand the lower threshold of conduction regime, experiments with even smaller beam diameters were carried out. In Fig. 13 examples of conduction welds achieved with small beam diameters are shown. Note that the welds with 0.07 mm beam diameter were achieved on a commercial powder bed machine, but no powder was used; just melting of the steel substrate. Unlike in Fig. 9 where it was not possible to achieve any melting with a beam diameter of 0.6 mm, here a pure conduction weld is shown for 0.1 mm beam and the same energy density of 4 kJ/cm² (Fig. 13a). This was possible due to decrease of interaction time from 120 ms to 2 ms and increase of power density from 33.1 kW/cm² to 2040 kW/cm². In the next example (Fig. 13b), it is shown that a conduction weld with an even smaller beam diameter could be achieved when an appropriately short interaction was used. In this case the interaction time was reduced to 0.05 ms and the power density increased to 5.2 MW/cm². A further increase of interaction time to 0.1 ms resulted in switching the process to keyhole regime, as shown in Fig. 13c. This suggests that the operating window for conduction regime is very narrow for this range of beam diameters.

4. Discussion

The main objective of this study was to investigate parameters that control the weld bead geometry in laser conduction welding. The first experiment examined if constant power density and specific point energy control the depth of penetration in conduction welding independently of the beam diameter, as reported for keyhole welding by Suder and Williams, (2012). The depth of penetration varied with beam

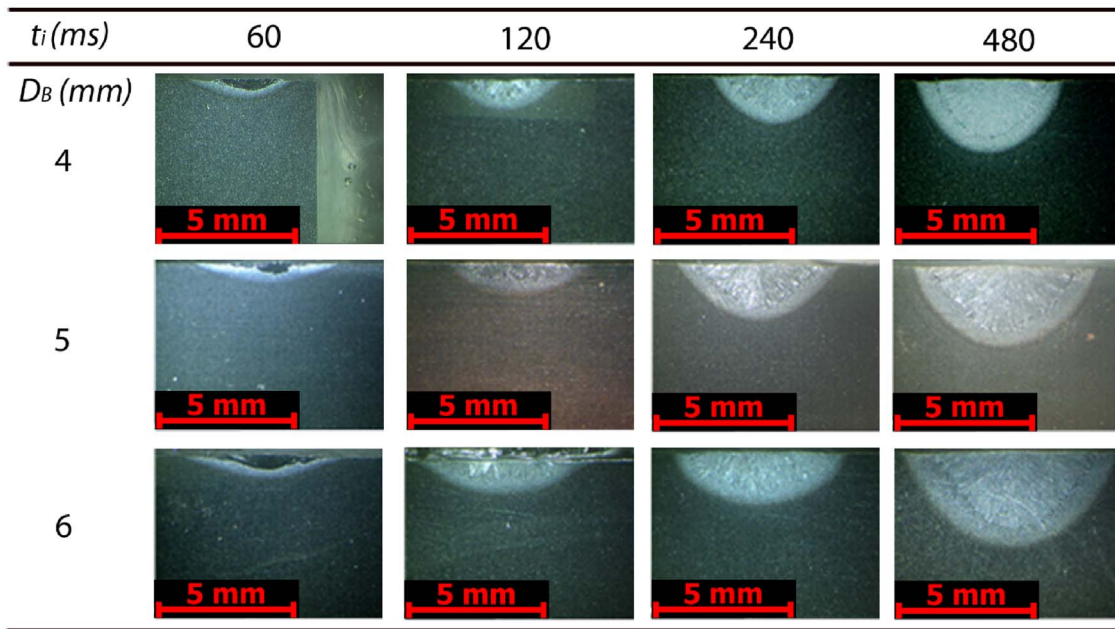


Fig. 6. Macrographs for different beam diameters and interaction times; constant power density of 28 kW/cm².

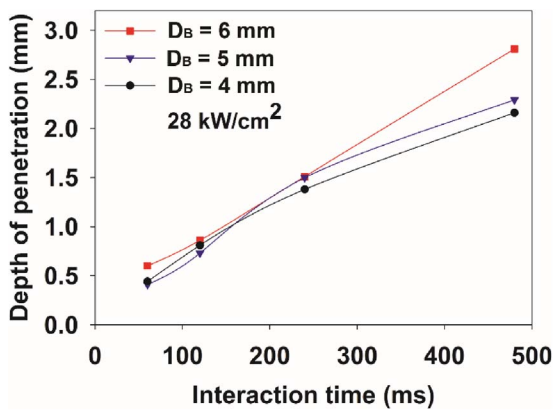


Fig. 7. Effect of interaction time on depth of penetration for different beam diameters and constant power density of 28 kW/cm² (Table 2).

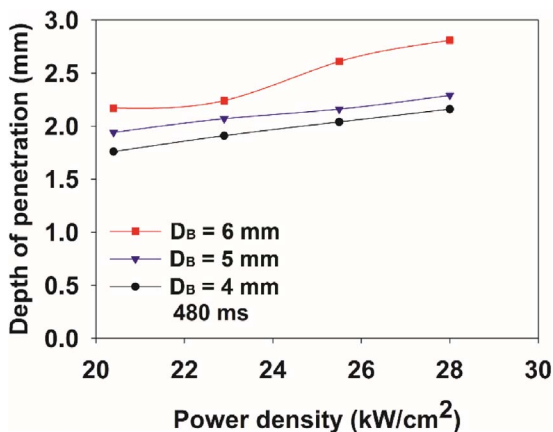


Fig. 8. Effect of power density on depth of penetration for different beam diameters and constant interaction time of 480 ms (Table 3).

diameter (Fig. 3), which is in contrast to keyhole welding. Conduction regime is controlled by the power density and interaction time, as shown in Fig. 5. This suggests significant differences in the response of the material between the two regimes. Keyhole regime is a vaporisation

driven process and hence the power density plays the most important role and the interaction time is less significant. As reported by [Suder and Williams, \(2012\)](#) the depth of penetration in keyhole regime is proportional to the power density and specific point energy. The specific point energy describes a discrete energy in a given laser size domain for a given interaction time in CW laser welding. In another means it defines the size of the domain over which a particular energy density is applied. Both the power density and the specific point energy determine the rate of vaporisation, which translates directly into the depth of a keyhole. In another paper [Suder and Williams, \(2014\)](#) have shown that depth of penetration is proportional to the power factor, which is a simplified product of power density and specific point energy. This shows that keyhole regime is a one dimensional process where the depth of penetration can be increased without increasing the weld width. In this case the laser power has to be increased only by a factor of two when the beam diameter is doubled to maintain constant depth of penetration. Similar correlation between the beam diameter and depth of penetration was found by [Patschger et al. \(2013\)](#), which supports this.

In conduction welding the energy has to be transferred into the material via conduction, which is a relatively slow process. As shown in [Figs. 7 and 8](#), the depth of penetration in conduction is strongly dependent on the interaction time (slope 0.94) and less dependent on the power density (slope 0.55). This is attributed to the process dynamics. There is a time required for the heat to conduct from the laser interaction point to the material and therefore the longer the interaction time the greater the size of the melt pool and weld depth. In conduction regime the response of penetration depth to the interaction time is greater than to the power density, provided that steady state conditions are achieved, i.e. sufficient energy density for melting is applied. There is a certain minimum power density and interaction time required to achieve melting. Therefore any change of interaction time at low power density will have no effect on the weld geometry, in the same way as any change of power density at short interaction time will not improve the depth of penetration, unless keyhole regime is induced. In addition, the different response of penetration depth to interaction time and power density, suggest that the process is not controlled by the energy density (the product of power density and interaction time). This assumption applies only to a narrow processing window and in other cases the power density and interaction time have to be considered separately.

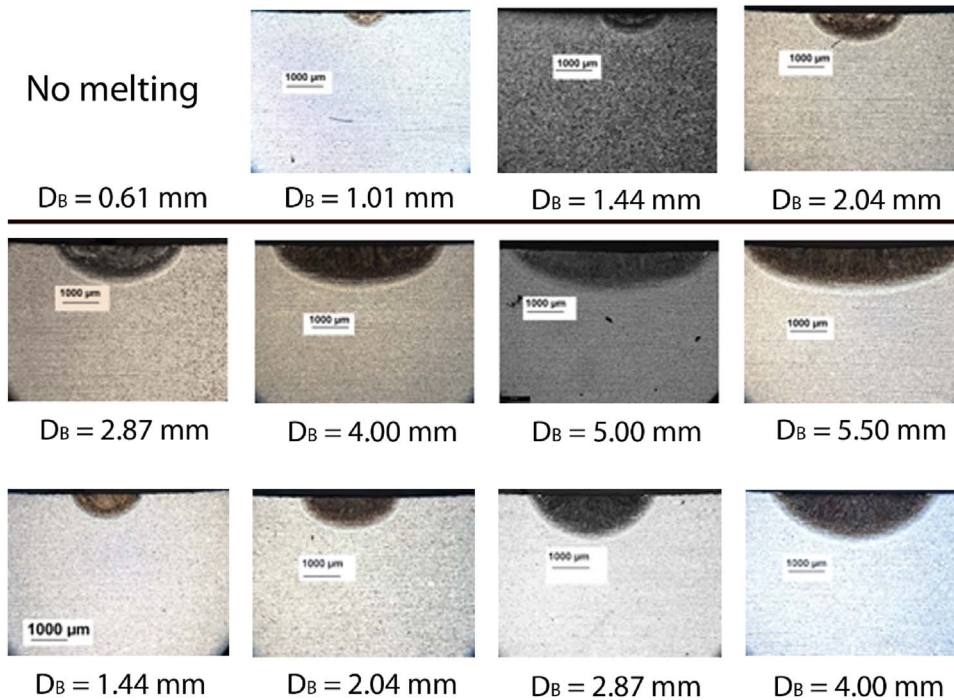


Fig. 9. Bead-on-plate welds produced at constant power density of 33.1 kW/cm² and interaction time of 120 ms, for a range of beam diameters.

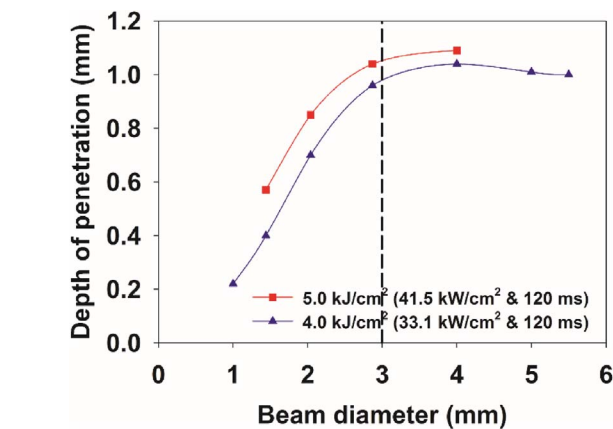


Fig. 11. Effect of beam diameter on depth of penetration at constant power density and interaction time.

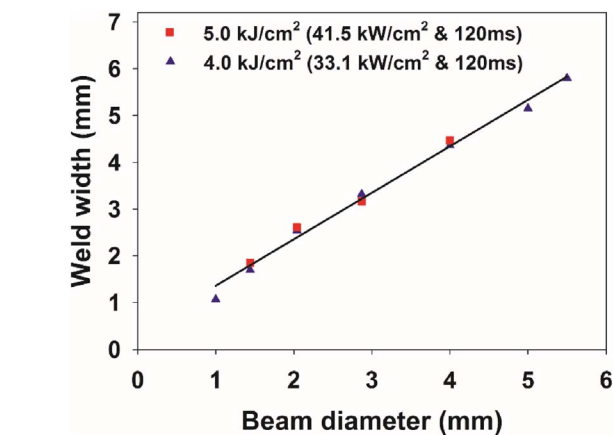


Fig. 12. Effect of beam diameter on weld width at constant power density and interaction time.

It seems that the weld profile in conduction regime is primarily controlled by the interaction time, but a certain minimum power density is also required to ensure melting. These two parameters control the

energy flux and the surface temperature. This means that to maintain a constant depth of penetration the laser power has to be quadrupled when the beam diameter increases by a factor of two. The beam diameter, on the other hand, controls the size of the domain over which the heat is applied and hence the weld width. Therefore the weld width in conduction welding is proportional to the beam diameter.

It was anticipated that the interaction time and power density could provide a simple phenomenological model to control the depth of penetration and the weld profile with variable beam diameters, similarly as the power factor in keyhole regime shown by Suder and Williams, (2014). However, as shown in Fig. 7 at longer interaction times (480 ms) the process is not independent of the beam diameter anymore. This can be attributed to the change of welding regime from conduction to transition or keyhole. This is shown in macrographs in Fig. 6, where all weld beads for the interaction time of 480 ms exhibit deeper profiles as it would result from pure conduction, which means that vaporisation was present. At longer interaction times the workpiece is exposed to the laser radiation for a longer time, thereby increasing the peak temperature. Thus, at a certain point the boiling point of a material will be exceeded leading to the change of a welding regime. This is shown in Fig. 14 where all data from Figs. 4 and 7 are plotted as a function of energy density. In conduction regime the process is independent of the beam diameter and all curves merge together, but at a certain point the beam diameter starts influencing the depth of penetration. At this point the transition regime commences and the vaporisation starts governing the process and the power density and specific point energy become dominant, as shown by Assuncao et al. (2012). This suggests that depending on the processing regime different parameters control the weld profile.

To investigate the effect of power density and interaction time ultimately, a further experiment on a wider range of beam diameters was carried out (). It turned out that the material response is not only dependent on the welding regime, but also on the range of beam diameters. Even in pure conduction regime the weld depth is dependent on the beam diameter when the beam is smaller than 2.9 mm (Fig. 11) at constant energy density. In this operating regime the process is not only controlled by the power density and interaction time, but also by the applied energy (specific point energy). This suggests that with small beams the process is less efficient than with big beams due to greater conduction losses.

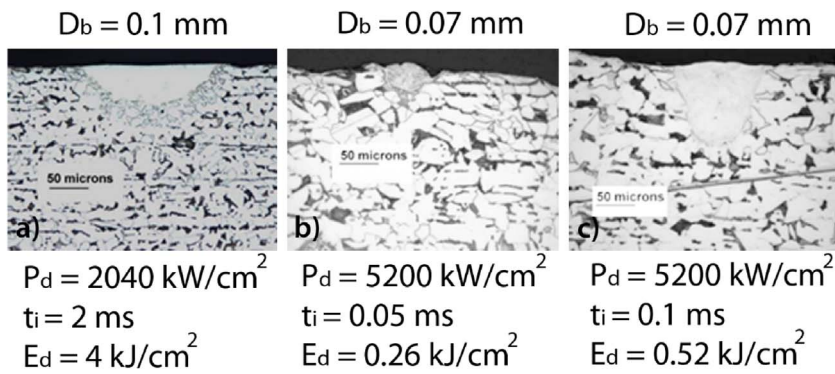


Fig. 13. Welds with small beam diameters; a,b) conduction regime, c) keyhole regime.

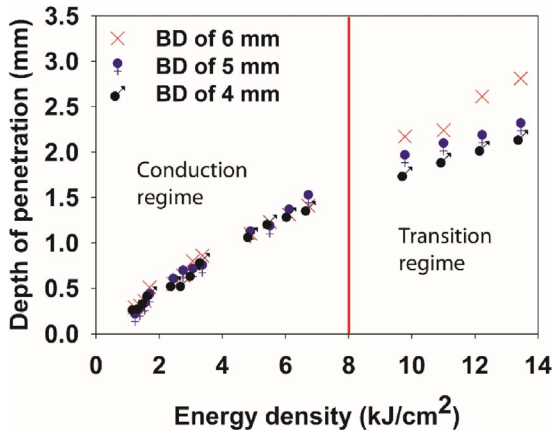


Fig. 14. Effect of energy density on depth of penetration in different welding regimes.

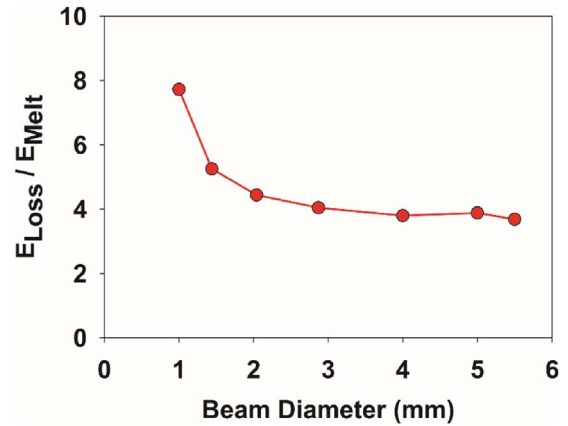


Fig. 16. Ratio of energy for melting to the energy for conduction losses calculated based on analytical heat equation (Eqs. (9) and 10).

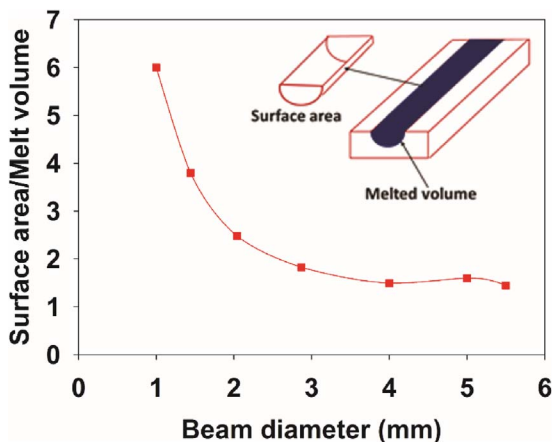


Fig. 15. Ratio of surface area to melt volume measured from macrographs in Fig. 9 (constant power density and interaction time) as a function of beam diameter.

A certain amount of energy is dissipated for the lateral thermal conduction into the bulk material. All the energy conducted into the workpiece, but not contributing to melting, is considered as a loss. These losses are proportional to the area of contact surface between the melt pool and the solid bulk material. The size of this surface is proportional to the size of the melt pool i.e. depth and width, which in pure conduction welding should have a constant ratio. The energy utilised for melting, on the other hand, is proportional to the melt volume. At a certain point, below a certain critical beam diameter, the conduction losses will be so high with respect to the applied energy that no melting of the material can occur, as shown in Fig. 9 for 0.6 mm beam diameter. This means that the ratio of energy dissipated in the bulk material to the energy utilised for melting decreases with increasing beam diameter. The ratio of the area of the contact surface to the melt volume measured

from macrographs in Fig. 9 is shown in Fig. 15. This ratio decreases rapidly, which corresponds to increase of process efficiency when the beam diameter is above two. This is the main reason why the process is more efficient with larger beams.

The relationship between the energy dissipated for conduction and the energy utilised for melting was calculated using an analytical solution of the heat equation, as described in Section 2.4. The area of melting ($T > 1500\text{ }^\circ\text{C}$) and the area of conduction losses ($1500 > T > 200\text{ }^\circ\text{C}$) were estimated from a one-dimensional temperature distribution (Eq. (7)). The ratio of energy loss to the energy utilised for melting for different beam diameters is shown in Fig. 16. The data confirm the hypothesis of a higher proportion of conduction losses for small beam diameters. This implies that it may be more difficult to achieve pure conduction welds with small beams. Any attempt to increase the input energy to overcome these losses is likely to result in vaporisation and keyhole regime. Therefore the change of processing regimes is expected to be more rapid with small beams.

One of the ways of reducing the heat losses in the bulk material and achieving conduction welds with small beam diameters is to decrease the interaction time. In this case the laser spot is interacting with a particular region of the material for a shorter period of time leading to a lower losses and a greater melting efficiency. Application of high power density but with short interaction time resulted in conduction welds, even with small beam diameters between 0.1–0.07 mm in Fig. 13a and b. Note that in the first case (Fig. 13a) the energy density was the same as in Fig. 9, but the combination of power density and interaction time different. The decrease of interaction time and increase of power density resulted in an increased rate of energy input, i.e. how fast the heat is applied and hence lower conduction losses in the bulk material. This proves that is possible to get conduction welds with such small beam diameters, but it is expected that the transition between keyhole and conduction regime is relatively narrow, which means that it is easy to exceed the energy required for vaporisation and induce keyhole regime,

as shown in Fig. 13c. The results indicate that with small beam diameters it is more difficult to achieve steady state conduction transfer due to low energy applied and high losses.

The depth of penetration in conduction welding is controlled by the power density and interaction time, provided that the ratio of the area of the contact surface of the melt-solid interface to the volume of liquid metal (Fig. 15) is below two. When this ratio increases above two, an additional energy is required to compensate for the higher conduction losses. In such an operating range, a short interaction time and a high power density are required to achieve melting, but the process control is more crucial due to the ease of inducing vaporisation.

5. Conclusions

Parameters controlling the weld profile in conduction laser welds were investigated. It has been shown that the depth of penetration in pure conduction welding is controlled by the power density and interaction time and is independent of the beam diameter, provided that energy is below the vaporisation threshold. Penetration depth is very dependent on the interaction time, because there is a minimum time required for the heat to conduct to the inner part of the material. Also the power density has to be high enough to ensure melting of the material. The weld width is proportional to the beam diameter, provided that the interaction time is long enough to allow for sufficient heat conduction.

For small beam diameters, the ratio between conduction losses and energy utilised for melting increases rapidly and the process becomes less efficient due to the geometrical aspects of the weld pool. Therefore below a certain ratio of the area of the melt-solid interface to the volume of the liquid metal, which is dependent on the beam diameter, the depth of penetration is not only controlled by the power density and interaction time, but it also depends on the specific point energy. This means that it is more difficult to achieve pure conduction welds with small beam diameters typically used in powder bed additive manufacturing and micro-welding, due to high losses and narrow transition between conduction and keyhole regimes.

Acknowledgements

This research was funded by EPSRC Centre for Innovative

Manufacturing in Laser based Production grant number EP/ J017086/ 1, SPI Lasers and Atomic Weapon Establishment UK. The authors are also grateful to Petroleum Technology Development Fund (PTDF) Nigeria for the student support. The authors thank Dr Ravi Aswathanarayanawamy of Renishaw PLC for producing the welds shown in Fig. 13 using the commercial powder bed machine. The underlying data can be accessed through the Cranfield University data repository at <https://doi.org/10.17862/cranfield.rd.5151301.v1>

References

- Ashby, M.F., Easterling, K.E., 1984. The transformation hardening of steel surfaces by laser beams-I: Hypo-eutectoid steels. *Acta Metall.* 32, 1935–1948.
- Assuncao, E., Williams, S., Yapp, D., 2012. Interaction time and beam diameter effects on the conduction mode limit. *Opt. Laser. Eng.* 50, 823–828.
- Bag, S., Trivedi, A., De, A., 2009. Development of a finite element based heat transfer model for conduction mode laser spot welding process using an adaptive volumetric heat source. *Int. J. Therm. Sci.* 48, 1923–1931.
- Benyounis, K.Y., Olabi, A.G., Hashmi, M.S.J., 2005. Effect of laser welding parameters on the heat input and weld-bead profile. *J. Mater. Process. Technol.* 164–165, 978–985.
- Buvanashakaran, G., Siva Shanmugam, N., Sankaranarayanan, K., Sabarikhant, R., 2009. A study of laser welding modes with varying beam energy levels. *Proc. Inst. Mech. Eng. Part C: J. Mech. Eng. Sci.* 223, 1141–1156.
- El-Batahy, A.M., 1997. Effect of laser welding parameters on fusion zone shape and solidification structure of austenitic stainless steels. *Mater. Lett.* 32, 155–163.
- Fuerschbach, P.W., Eisler, G.R., 2002. Effect of laser spot weld energy and duration on melting and absorption. *Sci. Technol. Weld. Join.* 7, 241–246.
- Meco, S., Pardal, G., Ganguly, S., Miranda, R.M., Quintino, L., Williams, S., 2013. Overlap conduction laser welding of aluminium to steel. *Int. J. Adv. Manuf. Technol.* 67, 647–654.
- Moradi, M., Ghoreishi, M., 2011. Influences of laser welding parameters on the geometric profile of Ni-base superalloy Rene 80 weld-bead. *Int. J. Adv. Manuf. Technol.* 55, 205–215.
- Mundra, M., Debroy, T., 1993. Toward understanding alloying element vaporization during laser beam welding of stainless steel. *Weld. Res. Suppl.* 1–9.
- Patschger, A., Gupner, M., Bliedtner, J., Bergmann, J.P., 2013. Remote micro welding with multi-mode and single-mode fiber lasers – a comparison. In: 32nd International Congress on Applications of Lasers and Electro-Optics. ICALEO, 2013. pp. 805–815.
- Sanchez-Amaya, J.M., Delgado, T., Gonzalez-Rovira, L., Botana, F.J., 2009. Laser welding of aluminium alloys 5083 and 6082 under conduction regime. *Appl. Surf. Sci.* 255, 9512–9521.
- Suder, W.J., Williams, S., 2012. Investigation of the effects of basic laser material interaction parameters in laser welding. *J. Laser Appl.* 24, 1–10.
- Suder, W.J., Williams, S., 2014. Power factor model for selection of welding parameters in CW laser welding. *Opt. Laser Technol.* 56, 223–229.